frontiers | Frontiers in Chemistry

TYPE Original Research
PUBLISHED 08 July 2024
DOI 10.3389/fchem.2024.1413489

OPEN ACCESS

EDITED BY
Yongjun Ji,
Beijing Technology and Business University, China

REVIEWED BY
Ivaylo Tankov,
Prof. Assen Zlatarov University, Bulgaria
Xupeng Zong,
Chinese Academy of Sciences, China
Jichang Lu,
Kunming University of Science and Technology, China

*CORRESPONDENCE
Guobo Li,
liguobo@ncu.edu.cn
Honggen Peng,
penghonggen@ncu.edu.cn

RECEIVED 07 April 2024
ACCEPTED 11 June 2024
PUBLISHED 08 July 2024

CITATION
Luo Y, He T, Li G, Wu D, Liu W, Zhang S and Peng H (2024), Synthetic Pt-Fe(OH)$_x$ catalysts by one-pot method for CO catalytic oxidation. *Front. Chem.* 12:1413489.
doi: 10.3389/fchem.2024.1413489

Synthetic Pt-Fe(OH)$_x$ catalysts by one-pot method for CO catalytic oxidation

Yiwei Luo[1,2], Tianyao He[3], Guobo Li[3]*, Daishe Wu[3], Wenming Liu[4], Shule Zhang[5] and Honggen Peng[3,4]*

[1]Jiangxi Acadmy of Eco-Environmental Science and Planning, Nanchang, Jiangxi, China, [2]Jiangxi Key Laboratory of Environmental Pollution Control, Nanchang, Jiangxi, China, [3]School of Resources and Environment, Nanchang University, Nanchang, Jiangxi, China, [4]School of Chemistry and Chemical Engineering, Nanchang University, Nanchang, Jiangxi, China, [5]School of Chemical Engineering, Nanjing University of Science and Technology, Nanjing, China

Catalytic oxidation is used to control carbon monoxide (CO) emissions from industrial exhaust. In this work, The prepared Pt$_a$-Fe(OH)$_x$ catalysts (x represents the mass fraction of Pt loading (%), a = 0.5, 1 and 2) by the one-pot reduction method exhibited excellent CO catalytic activity, with the Pt$_2$-Fe(OH)$_x$ catalyst, 70% and ~100% CO conversion was achieved at 30°C and 60°C, respectively. In addition, the Pt$_2$-Fe(OH)$_x$ catalyst also showed excellent H_2O resistance and hydrothermal stability in comparison to the Pt$_2$/Fe(OH)$_x$ catalyst prepared by impregnation method. Characterization results showed that the excellent catalytic performance of the catalysts was mainly attributed to the abundant surface oxygen species and Pt^0 the presence of H_2O, which promoted the catalytic reaction of CO, and Density functional theory (DFT) calculation showed that this was mainly attributed to the catalytic activity of the hydroxyl (-OH) species on Pt$_2$-Fe(OH)$_x$ surface, which could easily oxidize CO to -COOH, which could be further decomposed into CO_2 and H atoms. This study provides valuable insights into the design of high-efficiency non-precious metal catalysts for CO catalytic oxidation catalysts with high efficiency.

KEYWORDS

Fe(OH)$_x$ catalyst, hydroxyl (-OH) species, hydrothermal stability, density functional theory, mechanism

1 Introduction

Pt-based catalysts exhibit catalysts with excellent CO catalytic oxidation performance, but their performance usually tends to decrease significantly in the presence of H_2O (Lou and Liu, 2017; Li et al., 2024). Fe-based catalysts are a kind of non-precious metal CO catalytic oxidation catalysts with excellent performance (Zhang et al., 2015; Zheng et al., 2016; Haneda et al., 2017; Ma et al., 2020). The composite of Pt and Fe usually also exhibits excellent catalytic performance, Li et al. (2019) loaded Pt and Fe onto mesoporous Beta molecular sieves for the catalytic oxidation of CO, and the results showed that the Pt/(Fe^3)-mBeta catalysts showed the best catalytic activity, which was able to oxidize the CO completely at 90°C. Most importantly, the catalysts also showed excellent water resistance and stability, which was mainly attributed to the synergistic effect between the Pt/Fe valence and the large specific surface area of the catalysts. The self-inhibition of Pt metal particles by CO seriously impaired the catalytic oxidation performance of Pt-based catalysts, and the use of reducible metal oxides to load Pt metal particles is an effective method to avoid Pt self-

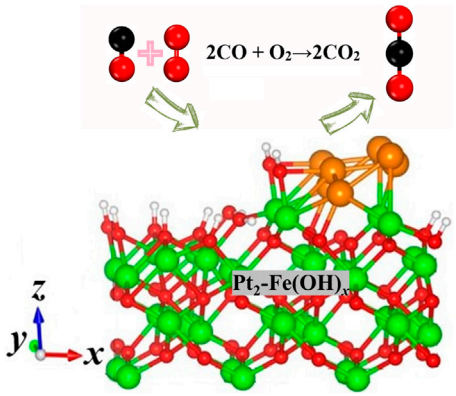

GRAPHICAL ABSTRACT

inhibition and improve the catalytic performance. Li et al. (2020) prepared a non-homogeneous Pt/Fe_3O_4 catalyst by *in situ* reduction of chloroplatinic acid on commercial Fe_3O_4 powders in ethylene glycol solution. Pt/Fe_3O_4 catalysts were prepared in ethylene glycol solution with non-homogeneous structure, and the non-homogeneous Pt/Fe_3O_4 catalysts had better CO catalytic oxidation performance compared with Fe_3O_4. For the Pt/Fe_3O_4 catalysts, the temperatures were 260°C and 290°C for 50% and 90% CO conversion, respectively, while for the Fe_3O_4 catalysts, the CO could only be completely oxidized when the temperature was higher than 310°C. The results showed that the Pt/Fe_3O_4 catalysts had better CO oxidation performance than the Fe_3O_4 catalysts. Characterization results showed that the metal Pt atoms have a strong synergistic effect with the Fe_3O_4 carrier, and the Pt metal particles promote the release of lattice oxygen and the formation of oxygen vacancies on Fe_3O_4, and the activation of oxygen molecules on the oxygen vacancies is the decisive step in the catalytic reaction. The effect of metal Fe, Co, Ni, Cu and Ce doping on the water resistance of Pt/Al_2O_3 catalysts was investigated by Tomita et al. (2014), and the results showed that iron oxide was the most effective promoter between −40°C and 150°C. The maximum CO conversion was observed at temperatures lower than 120°C with a molar ratio of 1 to Pt, and the CO conversion increased monotonically with Fe content at temperatures higher than 120°C. X-ray absorption fine-structure analysis showed that the formation of Pt-Fe alloys enhanced the CO oxidation activity at high temperatures but decreased it at low temperatures. Zhu et al. (2021) loaded Pt onto $CoFe_2O_4$ and $NiFe_2O_4$ spinel catalysts for the catalytic oxidation of CO, and found that the catalytic performance of Pt loaded onto spinel carriers was significantly better than that loaded onto single-metal-oxide carriers (e.g., Co_3O_4, Fe_2O_3, and NiO carriers), and the best catalytic activity was found with the TOF ranging from 0.27 to 1 s^{-1} at 50°C, which was higher than that of Pt/Fe_2O_4, which is three times higher than that of Pt/Fe_2O_3. The results showed that the strong interaction between Pt and spinel promoted the activation of oxygen species and weakened the adsorption of CO on Pt atoms, and the catalysts also showed good water resistance, even when the reaction conditions contained 10 vol% of H_2O vapour, the catalysts still maintained good catalytic performance, which is promising for the application of the catalysts. Wang et al. (2019) prepared carriers with different Cr/Fe ratios and loaded Pt for the catalytic oxidation of CO, and Pt/$Cr_{1.3}Fe_{0.7}O_3$ showed the best catalytic activity (conversion frequency of 0.2 s^{-1} at 80°C for 1% CO + 1% O_2), which was mainly attributed to its best reducibility. In addition, the catalyst remained highly active in the presence of 10% CO_2 and 10% H_2O vapor, and the kinetic results showed that CO_2 and H_2O have different effects on the catalytic reaction, with CO_2 competing with CO for adsorption and leading to the formation of carbonates, whereas H_2O promotes the decomposition of the carbonates, and that the promotion of H_2O is mainly due to the decrease in the strength of CO adsorption and the decrease in CO adsorption with CO, while H_2O promotes carbonate decomposition. In addition, the promotion of H_2O is mainly attributed to the weakening of CO adsorption and the rapid interfacial reaction between CO and the surface hydroxyl groups formed by the dissociation of H_2O. In addition, Pt-Fe-based catalysts are also commonly used for the preferential oxidation of CO under hydrogen-rich conditions. Prepared PtFe/CeO_2 catalysts for the preferential oxidation of CO using a one-pot method, and the Pt nanoparticles with a size of 2.8 nm were able to achieve CO conversion of 99.6% and CO_2 selectivity of 92.3% at room temperature, which meet the requirements for the preferential oxidation of CO under hydrogen-enriched conditions in fuel cell devices. The Pt nanoparticles were 2.8 nm in size.

A large number of research results have confirmed the existence of metal-oxide interfacial synergism between oxide carriers and noble metal nanoparticles, and Chen et al. (2014) constructed a Fe^{3+}-OH-Pt interface on the surface of Pt-Fe$(OH)_x$ composite nanoparticles, which significantly improved the CO oxidation activity of Pt-Fe$(OH)_x$ compared with that of traditional Pt metal nanoparticle catalysts. Density functional theory (DFT) calculation was carried out to investigate the mechanism of catalytic promotion at the Fe^{3+}-OH-Pt interface, and it was found that once CO was adsorbed on the Pt sites at the interface, it could be coupled with the adjacent OH to produce CO_2 after rapid dehydrogenation, which indicated that the OH at the interface was the active species for CO oxidation, after the desorption of CO_2, low-covalent Fe with ligand-unsaturated sites was generated at the interface, which could easily be adsorbed and activated. After the desorption of CO_2, low valent Fe is generated at the interface with unsaturated ligands, and these Fe sites can easily adsorb and activate O_2, and the activated oxygen species can oxidize the CO molecules adsorbed at the neighboring Pt

sites, and recover to the original Fe^{3+}-OH-Pt active interface with the aid of water vapour, so that the process can be recycled continuously.

In this work, the Pt and Fe species exhibited a good CO catalytic oxidation performance, and the hydroxyl species may have a favorable effect on the CO catalytic reaction. Based on the above results, Pt-Fe(OH)$_x$ rich in hydroxyl species was prepared by the *in situ* reduction one-pot method and used for the CO catalytic oxidation. The experimental results show that the catalysts not only have excellent catalytic performance, but also have good water-resistant performance.

2 Experimental section

2.1 Catalysts preparation

Preparation of Pt-(OH)$_x$ catalysts with hydroxyl species on the surface by one-pot method: add a fixed amount of $Fe(NO_3)_3{\cdot}9H_2O$ and H_2PtCl_6 into deionized water, stir to dissolve and mix well; while stirring, add NaOH solution (0.05 mol·L^{-1}) drop by drop into the above mixed solution, and stop the addition of NaOH solution (0.05 mol·L^{-1}), and then add 10 mL of KBH_4 (0.01 mol·L^{-1}) solution drop by drop to the above solution, and continuously stir for 3 h; centrifuge the suspension, wash and vacuum dry at 80°C; place the dried solid in an oven and dry at 150°C for 2 h to obtain Pt_a-Fe(OH)$_x$, and the loadings of Pt metal (a = 0.5%, 1% and 2%), respectively.

Preparation of contrast Pt/Fe(OH)$_x$ catalyst by impregnation method: A quantitative amount of $Fe(NO_3)_3{\cdot}9H_2O$ was added into deionized water, dissolved and mixed homogeneously with stirring; While stirring, NaOH solution (0.05 mol·L^{-1}) was added dropwise into the above mixed solution, and the addition was stopped when the pH was 9, and the stirring was continued for 3 h. The suspension was centrifuged and washed; The suspension was centrifuged, washed and vacuum dried at 80°C. The dried solid was placed in an oven; The dried solid was placed in an oven and dried at 150°C for 2 h to obtain Fe(OH)$_x$ carrier, and then was added to H_2PtCl_6 solution, stirred for 1 h, then added 10 mL of KBH_4 (0.01 mol·L^{-1}) solution drop by drop, and stirred continuously for 3 h; the suspension was centrifuged, washed and dried at 80°C. The dried solid was placed in an oven; The dried solid was placed in an oven and dried at 150°C for 2 h to obtain the Pt/Fe(OH)$_x$ catalyst.

2.2 CO catalytic oxidation activity evaluation

All evaluation experiments of the catalysts for CO catalytic oxidation were measured in a continuous flow fixed-bed reactor. To evaluate the effectiveness of internal diffusion, the Weisz-Prater Criterion was utilized. The CO catalytic oxidation activity was assessed using the standard reaction conditions: 50 mg catalyst, 1 vol% [CO], 21 vol% [O_2], N_2 as balance gas at a total flow rate of 30 mL·min^{-1}. The reactants and products were collected and examined using an N-2000 workstation and a GC9310 gas chromatograph, which was outfitted with a TDX-01 column and a TCD detector. The conversion of CO (X_{CO}) was calculated using Eq. 1:

$$X_{CO} = \left(1 - \frac{S_{CO\text{-}outlet}}{S_{CO\text{-}inlet}}\right) \times 100\% \quad (1)$$

where $S_{CO\text{-}outlet}$ and $S_{CO\text{-}inlet}$ are the CO concentrations in the inlet and outlet gas streams.

2.3 Catalyst characterization

The techniques, such as Transmission electron microscopy (TEM), H_2/NH_3-Temperature programmed reduction (TPR), and X-ray photoelectron spectroscopy (XPS) are carried out to characterize the obtained catalysts. Detailed description of the characterization procedure is in Supplementary Material.

2.4 DFT calculation details

The density functional theory calculations in this chapter were performed using the Vienna *ab initio* simulation package (VASP) software package, which describes the electron-ion interactions using the projected affixed wave (PAW) pseudopotential method. The truncation energy is 400 eV, and the exchange-correlation generalization is the GGA-PBE generalization. The description of the Fe 3d orbital electrons by the GGA generalization suffers from self-interaction errors, so it is corrected by the DFT + U method, with the value of U determined from the forbidden band width of Fe_2O_3 (Zhao et al., 2017). It was found that the calculated forbidden bandwidth of Fe_2O_3 is 2.02 for a U value equal to 4.6 eV, which agrees with the experimental value of 2.1 (Onoe et al., 2007), so the U value of 4.6 eV was used. For the spin-polarization calculations the magnetic properties of Fe were taken into account, and the use of a different spin orientation for Fe can have a significant effect on its energy, and all energy calculations were performed using an antiferromagnetic structure for the Fe atoms (Barnard and Guo, 2011). The structure chirality was calculated using a convergence criterion of all interatomic energies less than 10^{-4} eV and forces less than 0.05 eV. Brillouin zone integrals were calculated using the Monkhorst-Pack method using 3 × 2 × 1 K points. The lowest energy reaction path was calculated using the CI-NEB method, confirming the transition state structure by having only one imaginary frequency. A vacuum layer of 15 Å was set up to avoid interactions between repetitive slabs.

The structure was optimized with the bottom two layers of stoichiometric Fe_2O_3 fixed in the bulk lattice sites, and the top layer of Fe(OH)$_x$ and loaded Pt were fully chirped in the structure optimization and transition state calculations. Definition of adsorption energies of surface species: $E_{ads} = E_{adsorbate/catalyst} - E_{catalyst} - E_{adsordate}$, with $E_{adsorbate/catalyst}$, $E_{catalyst}$ and $E_{adsordate}$ representing free gas molecules, adsorbed Pt/Fe(OH)$_x$, substrate Pt/Fe(OH)$_x$ and the system energy, respectively.

3 Results and discussion

3.1 CO catalytic oxidation activity performance

The CO oxidation performance of the Fe(OH)$_x$, Pt_2/Fe(OH)$_x$ and Pt_2-Fe(OH)$_x$ catalysts is shown in Figure 1A. The Fe(OH)$_x$ catalyst without active component Pt loading showed a poor CO catalytic performance, CO could only be completely oxidized at 220°C. As the Fe(OH)$_x$ catalyst were loaded with 2 wt% Pt by two methods (Pt_2/Fe(OH)$_x$ by Wet-impregnation: and Pt_2-Fe(OH)$_x$ by one-pot reduction), CO oxidation was improved significantly. As

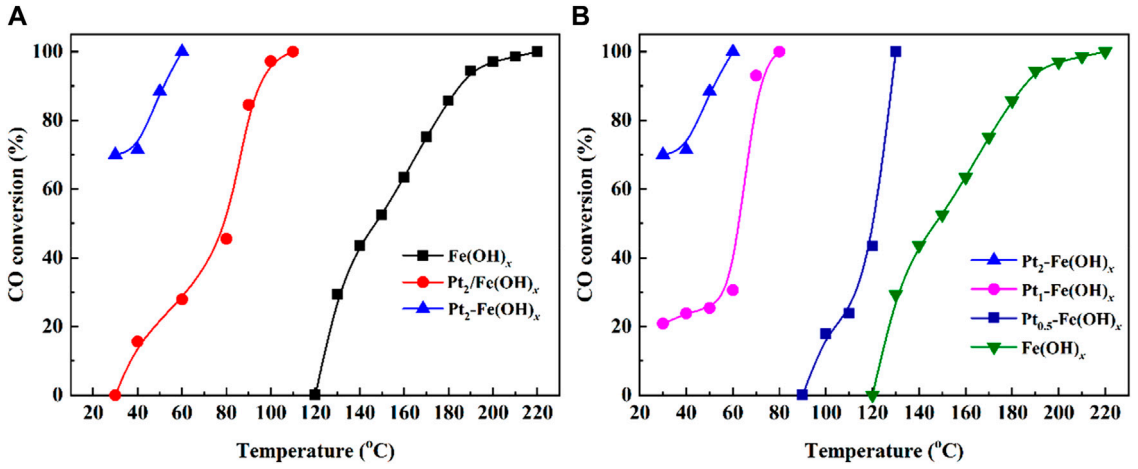

FIGURE 1
CO catalytic oxidation performance of **(A)** $Fe(OH)_x$, $Pt_2/Fe(OH)_x$ and Pt_2-$Fe(OH)_x$, **(B)** Pt_a-$Fe(OH)_x$ (a = 0.5, 1, and 2) catalysts.

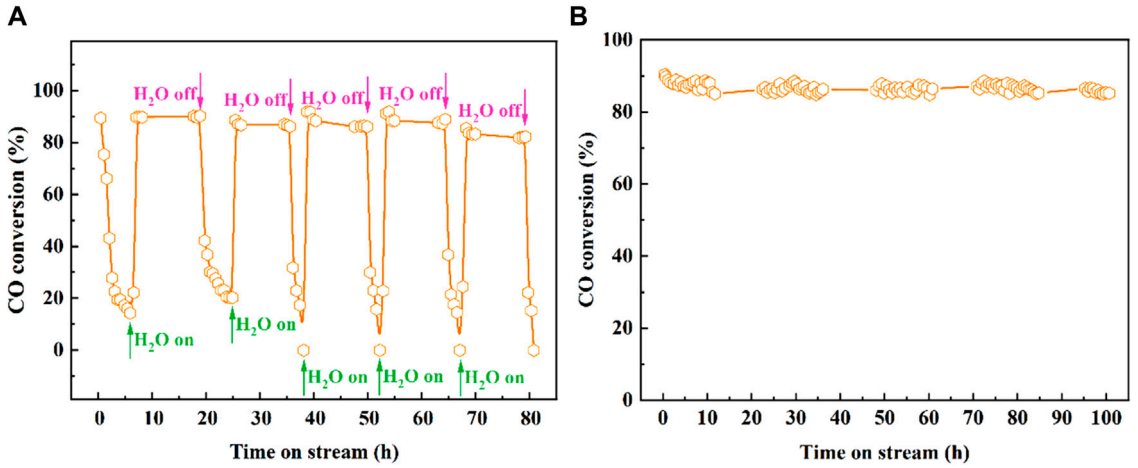

FIGURE 2
CO catalytic oxidation performance with 3.0 vol% H_2O of Pt_2-$Fe(OH)_x$ catalyst **(A)** five reaction cycles, **(B)** stability of Pt_2-$Fe(OH)_x$ catalyst at 50°C.

can be seen, in particular Pt_2-$Fe(OH)_x$, which was obtained via the one-pot reduction method, showed the best CO catalytic activity (the CO conversion could reach 70% only at 30°C). Furthermore, the CO catalytic oxidation efficiency of Pt_a-$Fe(OH)_x$ (a = 0.5, 1 and 2) catalyst with different Pt contents was further evaluated, the results was shown in Figure 1B, the CO catalytic performance of the catalysts decreases when the loading of Pt is decreased, and the complete CO oxidation temperatures of Pt_1-$Fe(OH)_x$ and $Pt_{0.5}$-$Fe(OH)_x$ are 80°C and 130°C, respectively. Thus, the Pt_2-$Fe(OH)_x$ is the most potential CO catalytic oxidation catalyst.

3.2 CO catalytic oxidation stability evaluation

The H_2O resistance and long-time stability of the catalysts are crucial, and the stability test of Pt_2-$Fe(OH)_x$ catalyst is exhibited in Figure 2. As shown in Figure 2A, the Pt_2-$Fe(OH)_x$ catalyst has a high initial CO catalytic oxidation activity at 50°C (the CO conversion reaches about 90%), while the CO catalytic activity decreases significantly with the extension of the reaction time, and after 6 h, the CO conversion decreases to about 14%. Interestingly, when 3.0 vol% of H_2O was introduced into the reaction gas, the CO catalytic activity was sharply enhanced, and the CO conversion increased from 14% to about 90% within a short time, and the CO catalytic activity remained unchanged within 10 h. When the H_2O in the reaction gas was withdrawn, the CO conversion decreased steeply to about 20% after 6 h, and then the CO conversion rate decreased to about 20% after 3.0 vol% of water vapor was introduced into the reaction gas again. When 3.0 vol% of H_2O was introduced to the reaction system, the CO catalytic activity of Pt_2-$Fe(OH)_x$ catalyst was restored to the initial state, and the catalytic performance remained similar after five reaction cycles. The obtained results showed that water vapor significantly promoted the catalytic

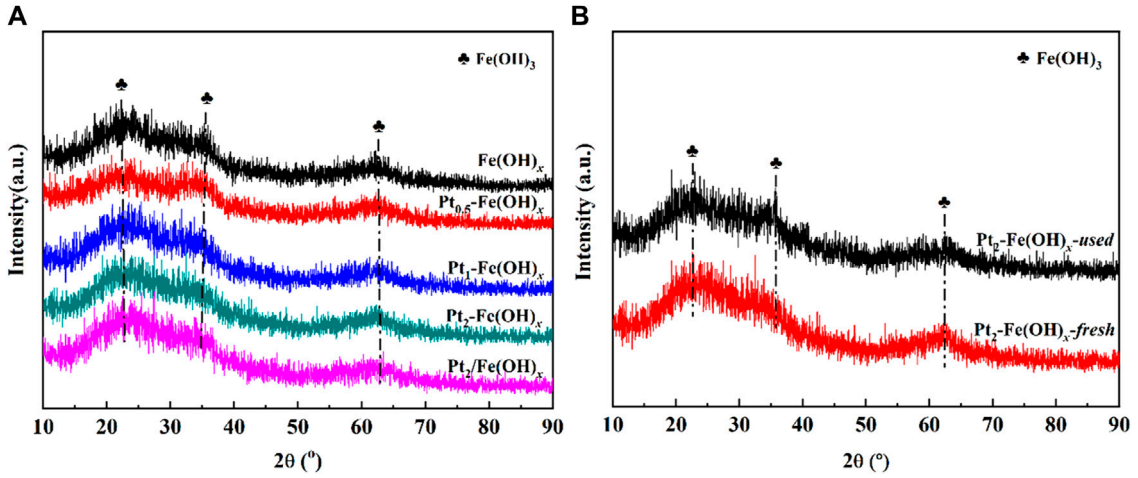

FIGURE 3
XRD spectrum of **(A)** $Fe(OH)_x$, Pt_a-$Fe(OH)_x$ and $Pt_2/Fe(OH)_x$, **(B)** fresh and used Pt_2-$Fe(OH)_x$ catalysts.

performance of Pt_2-$Fe(OH)_x$ catalyst, and the catalysts possessed excellent H_2O resistance, which might be related to the hydroxyl (-OH) species involved in the reaction on the catalyst surface. In addition, the catalytic stability was tested for a long time, and the results are shown in Figure 2B. The CO catalytic activity of the Pt_2-$Fe(OH)_x$ catalyst was almost unchanged and remained at about 85% for 100 h of stability test with 3 vol% H_2O. The obtained results show that the Pt_2-$Fe(OH)_x$ catalyst exhibited excellent H_2O resistance and hydrothermal stability. The CO catalytic oxidation reaction pathway was assumed as: ① $CO_{free} \rightarrow CO_{ads}$, ② $CO_{ads} + O_{lat} \rightarrow CO_{2free} + O_{vac}$, ③ $H_2O_{free} + O_{lat} \rightarrow OH_{ads} + OH_{lat}$, ④ $CO_{ads} + OH_{ads} \rightarrow COOH$, and ⑤ $COOH + OH_{lat} \rightarrow CO_{free} + H_2O_{free} + O_{vac}$. In which, the subscript of $_{free}$ and $_{ads}$ denoted the free and adsorbed state species, respectively. In addition, the oxygen vacancy (O_{vac}) structure generated during the reaction may in dynamic equilibrium, i.e., what is consumed is replenished in a timely regeneration.

3.3 XRD, TEM and vacuum infrared spectroscopy analysis

The obtained XRD results of the catalysts are shown in Figure 3. It can be seen from Figure 3A that the $Fe(OH)_x$, Pt_a-$Fe(OH)_x$ and $Pt_2/Fe(OH)_x$ catalysts after drying at 150°C all showed the characteristic diffraction peaks of $Fe(OH)_3$, which indicated that the catalyst carriers mainly existed in the form of $Fe(OH)_3$ at this temperature. Figure 3B shows the XRD spectrum of the catalyst after the reaction, the catalyst still exhibits the typical characteristic diffraction peaks of $Fe(OH)_3$, which indicates that the composition of the catalyst does not change. In addition, the characteristic diffraction peaks for Pt were not detected for the fresh Pt-containing catalysts, which was mainly attributed to the low or highly dispersed Pt active component, and the characteristic diffraction peaks for the reacted catalysts were not detected, which indicated that the Pt species did not grow up agglomerated. $Fe(OH)_3$ has a large number of hydroxyl species, and the Pt species can be highly dispersed on $Fe(OH)_3$ without sintering and aggregation for a long time, which is an important factor for the excellent catalytic performance of the $Pt_2/Fe(OH)_x$ catalysts prepared by the one-pot reduction method.

Transmission electron microscopy (TEM) characterization of the Pt_2-$Fe(OH)_x$ catalyst is shown in Supplementary Figure S1. For the Pt_2-$Fe(OH)_x$ catalyst prepared by the one-pot reduction method, a lattice fringe of 0.23 nm was detected, which corresponds to the (111) crystalline plane of the Pt metal; however, no lattice fringe was detected with respect to the Pt species for the Pt_2-$Fe(OH)_x$ catalyst prepared by the impregnation method. This suggests that the preparation method influences the form of Pt species present in the catalyst, which in turn influences the catalytic activity of the catalyst.

The vacuum infrared spectroscopy of fresh and used Pt_2-$Fe(OH)_x$ catalysts is shown in Supplementary Figure S2, in which the peak at 3,389 cm^{-1} is corresponding to characteristic peak of hydroxyl species on the catalysts surface. It can be seen that the intensity of the peak of the hydroxyl species of the catalyst decreased significantly after the reaction, which indicates that the hydroxyl species were gradually consumed with the reaction, which is the main factor for the decrease of the catalyst performance. When 3.0 vol% H_2O was introduced into the reaction gas, it was beneficial to compensate for the depleted hydroxyl species on the catalyst surface, so the catalytic activity of the catalyst could be recovered rapidly.

3.4 XPS and H_2-TPR results analysis

The CO catalytic oxidation reaction takes place on the catalyst surface, so it is crucial to explore the chemical properties and composition information of surface species. The obtained Pt 4f orbitals XPS spectra of the catalysts are shown in Figures 4A, B, and the presence of Pt^0 and Pt^{2+} can be detected for the Pt_2-$Fe(OH)_x$ (Pt^0/Pt ratio is 0.69) prepared by the one-pot reduction method and for the $Pt_2/Fe(OH)_x$ (Pt^0/Pt ratio is 0.30) catalysts prepared by the

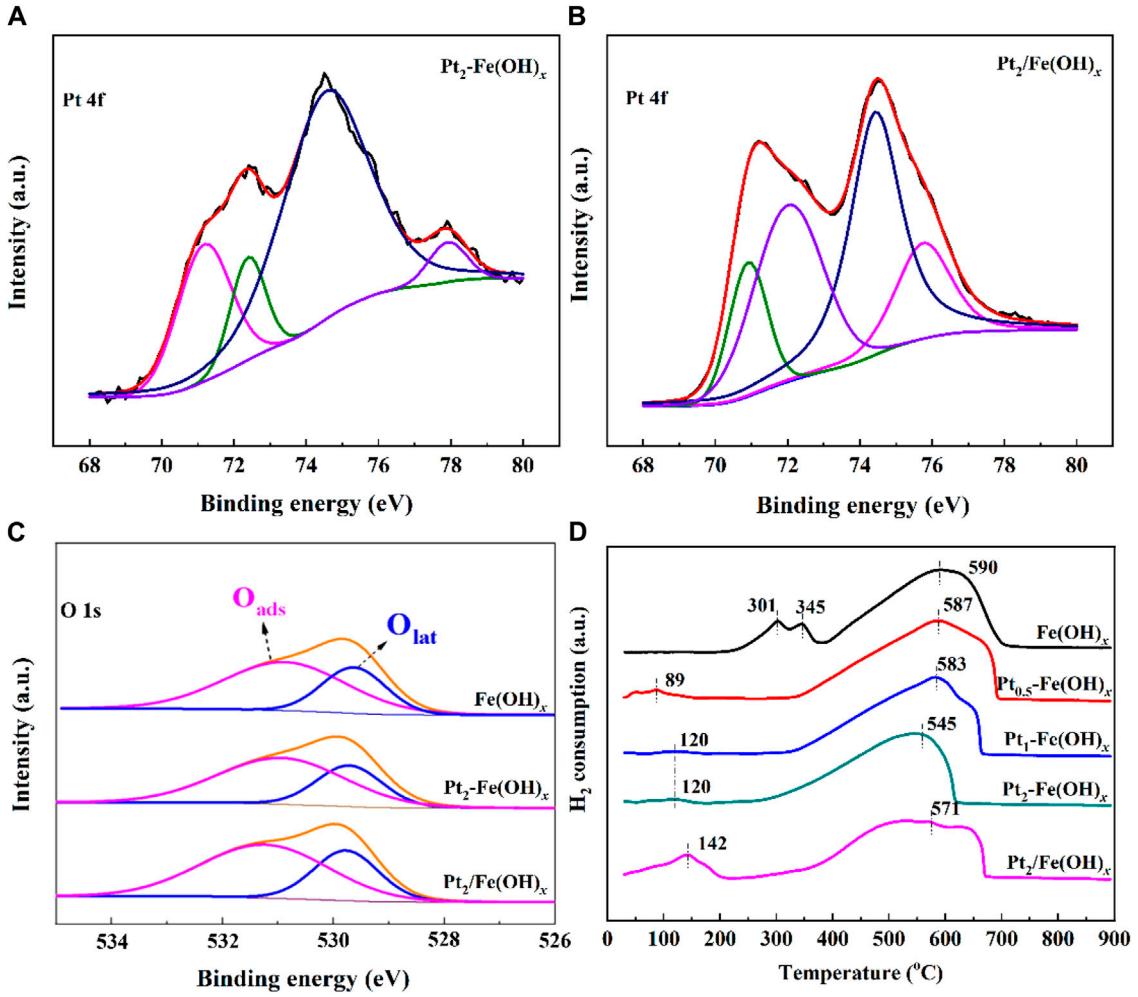

FIGURE 4
(A–C) XPS spectra and **(D)** H_2-TPR results of catalysts.

TABLE 1 Quantitative XPS peak results of the catalysts.

Catalysts	BE of Pt $4f_{7/2}$ (eV)		BE of O $1s_{3/2}$ (eV)		Pt^0/Pt	Oads/Olat
	Pt^0	Pt^{2+}	O_{ads}	O_{lat}		
Fe(OH)*x*	—	—	530.9	529.9	—	2.09
Pt_2-Fe(OH)*x*	71.2	72.4	531.0	529.7	0.69	2.11
Pt_2/Fe(OH)*x*	70.9	72.1	531.3	529.8	0.30	1.98

impregnation method (Oi-Uchisawa et al., 2003; Rohrbach et al., 2004), and the quantitative results, as shown in Table 1, indicate that Pt_2-Fe(OH)$_x$ has the most Pt^0, i.e., the one-pot reduction method is favorable for the reduction of Pt species, which is consistent with the TEM results of the catalysts. Moreover, numerous studies have shown that Pt^0 is more favorable for the catalytic oxidation of CO compared with Pt^{2+}. As shown in Figure 4C, the catalyst surface exhibited two kinds of oxygen species (the surface adsorption oxygen species (O_{ads}), which are mainly hydroxyl species, and the lattice oxygen (O_{lat}) species) (Si et al., 2020; Su et al., 2020; Xiong et al., 2020; Yang et al., 2020). Quantitative results show that Pt_2-Fe(OH)$_x$ has the most surface oxygen species (the O_{ads}/O_{lat} ratio is 2.11), higher than that of Pt_2/Fe(OH)$_x$ (the O_{ads}/O_{lat} ratio is 1.98), indicating that it has the most surface hydroxyl species, which is consistent with the best CO catalytic oxidation activity.

The results of the H_2-TPR curves of the catalysts are shown in Figure 4D, with the reduction peaks at 90–150°C attributed to the reduction of Pt species, and the reduction peaks at 300–600°C attributed to the reduction of $Fe(OH)_3$ species. Compared with

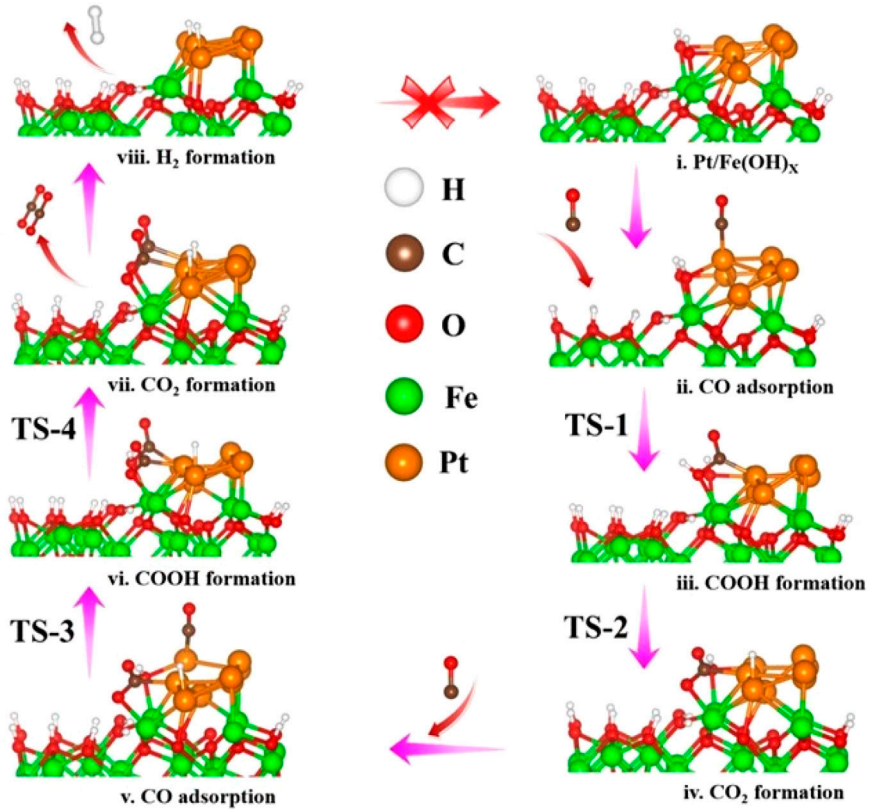

FIGURE 5
Reaction mechanism process of H_2 on Pt-Fe(OH)$_x$ surface. **(i)** Pt/Fe(OH)*x* **(ii)** CO adsorption **(iii)** COOH formation **(iv)** CO_2 formation **(v)** CO adsorption **(vi)** COOH formation **(vii)** CO_2 formation **(viii)** H_2 formation.

the carrier Fe(OH)$_x$, the Fe(OH)$_3$ of Pt$_2$-Fe(OH)$_x$ species prepared by the one-pot reduction method was shifted towards lower temperatures, suggesting that the introduction of Pt could improve the oxidation capacity. In addition, the reduction peak temperature of the Pt element in Pt-Fe(OH)$_x$ was shifted to the low temperature direction compared with that of the Pt$_2$/Fe(OH)$_x$ catalyst prepared by impregnation method, which indicated the improvement of the oxidation capacity of the catalyst, and this was one of the reasons for the better CO catalytic oxidation performance of the Pt$_2$-Fe(OH)$_x$ catalyst prepared by the one-pot method.

3.5 Density functional theory (DFT) results analysis

3.5.1 The optimized DFT calculation structures

The Pt-Fe(OH)$_x$ catalyst was successfully synthesized and TEM characterization confirmed that Pt exposed crystalline surface as (111) and XRD diffraction surface carrier as α-Fe$_2$O$_3$. Experimental and theoretical calculations pointed out that H_2O dissociates readily on the surface of α-Fe$_2$O$_3$. Theoretical calculations by Nguyen et al. (2013) showed that Fe-O3-Fe as the terminals is the most stable surface, and that the dissociation of H_2O into OH and H on the surface exotherms 0.25 eV. The dissociation energy barrier calculated by NEB is only 0.06 eV, which is almost negligible. It is proved that H_2O can be easily dissociated on the surface of α-Fe$_2$O$_3$ H_2O is easily dissociated on the surface of α-Fe$_2$O$_3$ (0001) at room temperature, and the dissociated H atoms can easily form OH with the unsaturated O atoms on the surface to form surface hydroxylation. OH with the unsaturated O atoms on the surface, forming Fe(OH)$_x$ with surface hydroxylation.

The interface of Fe(OH)$_x$ surface loaded with Pt is simulated by constructing periodic one-dimensional pt nanoribbons along the b-direction of the Fe(OH)$_x$ surface. As shown in Supplementary Figure S3A (the optimized Pt-Fe$_2$O$_3$ structure), the α-Fe$_2$O$_3$(0001) surface adopts a *p* (3 × 2) supercell containing three layers of Fe$_2$O$_3$ with stoichiometric number (each layer contains 12 Fe atoms and 18 O atoms), and the continuous monolayer Pt nanoribbon along the y-direction contains 8 Pt atoms, and DFT calculations indicate that the 8 Pt can be stably anchored on the α-Fe$_2$O$_3$ (0001) surface,. The average bond energy per Pt atom is 1.89 eV/Pt. As shown in Supplementary Figure S3B [the optimized Pt-Fe(OH)$_x$ structure], the Fe(OH)$_x$ surface is formed by saturating the exposed O atoms in the outermost layer of α-Fe$_2$O$_3$(0001) with H atoms to form OH, and two OHs adsorbed at the bridge between Fe and Pt are dissociated from H_2O. The surface OH/O is 1.5, which is consistent with our XPS results. The involvement of H_2O in the CO oxidation process to elucidate, DFT was used to investigate the role of hydroxyl group (-OH) in CO oxidation.

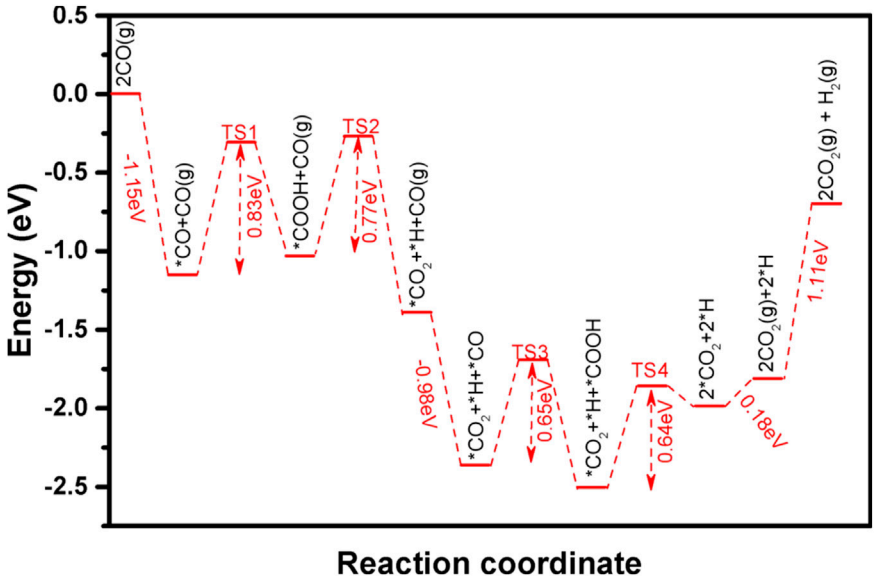

FIGURE 6
Intermediate species and energy barrier changes for CO oxidation on the Pt-Fe(OH)$_x$ surface.

3.5.2 Oxidation of the first CO molecule on the Pt-Fe(OH)$_x$ surface

The -OH species on Pt-Fe(OH)$_x$ surface are readily accessible through H_2O dissociation, and thus the adsorbed CO is susceptible to coupling with the OH at the interface, triggering the oxidation of CO. Figure 5i shows the reaction of the first adsorbed CO on the Pt-Fe(OH)$_x$ interface with the coupled OH, and the transition state structure TS-1 is shown in Supplementary Figure S4. The initial state is CO adsorbed on the slant top site of Pt with an adsorption energy of −1.15 eV, and CO is activated on the Pt surface (Figure 5ii). The distance between the O-atom of OH and the C-atom of CO is 3.050 Å. The bond length of O-Pt is 2.221 Å and that of C-Pt is 1.859 Å. Our calculations give the reaction of co-adsorbed -OH and CO to form -COOH (Figure 5iii), with a heat uptake of 0.12 eV and an activation energy base of 0.83 eV (Figure 6). This is consistent with the energy barrier for the formation of -COOH on the Fe(III)-OH-Pt surface OH with CO calculated by Zhao et al. (2014). The generated -COOH is adsorbed between Pt and Fe with a C-Pt bond length of 1.974 Å, and the distance between the O-atom of -OH and Fe is 2.233 Å. The O-H bond of -COOH is activated, and -COOH can easily dissociate further to CO_2 and H. The H-atom is detached from -COOH to the apical position of the Pt atom on the surface, and the H-Pt bond is 1.561 Å long (Figures 5iv, vi, viii). The H-Pt bond is 1.561 Å long (Figure 5iv), and its transition state structure TS-2 is shown in Supplementary Figure S4. The process is exothermic −0.38 eV, and the activation energy barrier for the reaction is 0.77 eV (Figure 6). After shedding the H atoms, the remaining molecular CO_2 is weakly adsorbed between Pt and Fe. Gong et al. (2003) calculated that it is relatively difficult to dissociate -COOH into CO_2 and H atoms from 3 layers of Pt (111) on the surface, with an energy barrier of E_a = 1.02 eV, which is 0.25 eV higher compared to ours, suggesting that the incorporation of the Fe(OH)$_x$ carrier facilitates the dissociation of -COOH.

3.5.3 Oxidation of a second CO molecule on the Pt-Fe(OH)$_x$ surface

Similarly, the second CO oxidation process was explored. Its CO is also adsorbed on the Pt at the slant top site (Figure 5v), with an adsorption energy of −0.98 eV. Like the mechanism of the first CO oxidation, the adsorbed CO reacts with the OH adsorbed on the bridge sites of Pt and Fe to form -COOH (Figure 5vi), and the transition structure TS-3 is shown in Supplementary Figure S4. Unlike the first CO oxidation, the second CO oxidation is exothermic at 0.15 eV, with an activation barrier of 0.65 eV (Figure 6). The second CO oxidation is thermodynamically and kinetically more favorable than the first CO oxidation, demonstrating that the presence of weakly adsorbed CO_2 on the surface is conducive to the formation of -COOH from CO and OH, and the stable presence of -COOH, which also readily desorbs an H atom onto Pt, forms a second weakly adsorbed CO_2, the transition state structure TS-4 as shown in Supplementary Figure S4, which is thermally adsorptive, with a reaction activation barrier of 0.50 eV and an activation energy barrier of 0.64 eV. Like the first CO oxidation process, CO oxidation is also an OH-consuming process.

In summary, the detailed CO catalytic oxidation pathway on Pt-Fe(OH)$_x$ surface is: Fe(OH)$_x$ surface is: ① 2 $CO_{free} \rightarrow CO_{free} + CO_{ads}$, ② $CO_{free} + CO_{ads} + OH \rightarrow COOH_{ads} + CO_{free}$, ③ $COOH_{ads} + CO_{free} \rightarrow CO_{2ads} + H_{ads} + CO_{free}$, ④ $CO_{2ads} + H_{ads} + CO_{free} \rightarrow CO_{2ads} + H_{ads} + CO_{ads}$, ⑤ $CO_{2ads} + H_{ads} + CO_{ads} + OH \rightarrow CO_{2ads} + H_{ads} + COOH_{ads}$, ⑥ $CO_{2ads} + H_{ads} + COOH_{ads} \rightarrow 2CO_{2ads} + 2H_{ads}$, ⑦ $2CO_{2ads} + 2H_{ads} \rightarrow 2CO_{2free} + 2H_{ads}$ and ⑧ $2CO_{2ads} + 2H_{ads} \rightarrow 2CO_{2free} + H_{2free}$.

3.5.4 Desorption of CO_2 and formation of H_2

The two CO_2 adsorbed weakly on the surface and released as gaseous CO_2 only need to overcome an energy of 0.18 eV, which can be easily desorbed from the Pt-Fe(OH)$_x$ surface at room temperature. The activation of the two H atoms adsorbed on the Pt surface to form gaseous H_2 needs to overcome an energy of 1.11 eV. Dreyer et al. (2015) calculated by DFT the energy of adsorption of dissociative H_2 on the Pt-

Fe_2O_3 surface to be E_{ads} = −117.7 KJ/mol, which is consistent with the DFT calculation results for the formation of H_2. The theoretical calculations indicate that there is a water-gas reaction on the Pt-$Fe(OH)_x$ surface, which leads to the depletion of surface -OH. Chen et al. (2018) experimentally concluded that the Pt-FeO_x surface undergoes water-gas reaction.

3.6 Conclusion

In this work, the prepared Pt_a-$Fe(OH)_x$ catalysts (a represents the mass fraction of Pt loading (%), a = 0.5, 1 and 2) by the one-pot reduction method exhibited excellent CO catalytic activity, with the Pt_2-$Fe(OH)_x$ catalyst, 70% and ~100% CO conversion was achieved at 30°C and 60°C, respectively. In addition, the Pt_2-$Fe(OH)_x$ catalyst also showed excellent H_2O resistance and hydrothermal stability in comparison to the Pt_2/$Fe(OH)_x$ catalyst prepared by impregnation method. Characterization results showed that the excellent catalytic performance of the catalysts was mainly attributed to the abundant surface oxygen species and Pt^0 the presence of H_2O, which promoted the catalytic reaction of CO. A combination of *in situ* DRIFTS and DFT calculations was used to establish the detailed catalytic CO removal pathway on Pt-$Fe(OH)_x$ surface, that is: ① $2\,CO_{free} \rightarrow CO_{free} + CO_{ads}$, ② $CO_{free} + CO_{ads} + OH \rightarrow COOH_{ads} + CO_{free}$, ③ $COOH_{ads} + CO_{free} \rightarrow CO_{2ads} + H_{ads} + CO_{free}$, ④ $CO_{2ads} + H_{ads} + CO_{free} \rightarrow CO_{2ads} + H_{ads} + CO_{ads}$, ⑤ $CO_{2ads} + H_{ads} + CO_{ads} + OH \rightarrow CO_{2ads} + H_{ads} + COOH_{ads}$, ⑥ $CO_{2ads} + H_{ads} + COOH_{ads} \rightarrow 2CO_{2ads} + 2H_{ads}$, ⑦ $2CO_{2ads} + 2H_{ads} \rightarrow 2CO_{2free} + 2H_{ads}$ and ⑧ $2CO_{2ads} + 2H_{ads} \rightarrow 2CO_{2free} + H_{2free}$. Two CO and -OH on the surface of Pt-$Fe(OH)_x$ form -COOH with reaction barriers of 0.83 and 0.65 eV, respectively, which indicates that the -OH on the surface of Pt-$Fe(OH)_x$ has a better activity and can easily oxidize CO to -COOH, which can be further detached to CO_2 and H atoms, with reaction barriers of 0.77 and 0.65 eV, respectively. The existence of H_2O reaction on the surface of Pt-$Fe(OH)_x$ that H_2O decomposes into H and -OH, and the combination of -OH and CO into -COOH leads to the depletion of the -OH on the surface of Pt-$Fe(OH)_x$. If there is no H_2O added continuously during the reaction, the -OH is not replenished, and there is no -OH to participate in the oxidation of CO, the catalyst activity will be decreased, which is consistent with the activity of our catalyst, i.e., the activity is decreased when we withdraw H_2O, and the activity is recovered when -OH is replenished after H_2O is added. This study holds significance for further understanding the application potential of nano-catalysts in important oxidation reactions and provides valuable insights for the development of efficient CO oxidation catalysts.

Data availability statement

The original contributions presented in the study are included in the article/Supplementary Material, further inquiries can be directed to the corresponding authors.

Author contributions

YL: Data curation, Formal Analysis, Methodology, Writing–original draft, Writing–review and editing. TH: Investigation, Methodology, Writing–review and editing. GL: Funding acquisition, Project administration, Supervision, Writing–review and editing. DW: Investigation, Methodology, Writing–review and editing. WL: Investigation, Methodology, Writing–review and editing. SZ: Supervision, Writing–review and editing. HP: Funding acquisition, Project administration, Supervision, Writing–review and editing.

Funding

The author(s) declare that financial support was received for the research, authorship, and/or publication of this article. This work was supported by the National Key R&D Program of China (2023YFB3810801), National Natural Science Foundation of China (22276086 and 22306086), the Natural Science Foundation of Jiangxi Province (20202ACB213001, 20232BCJ22003 and 20232BAB213028), the National Engineering Laboratory for Mobile Source Emission Control Technology (NELMS2019A12), the State Key Laboratory of Clean Energy Utilization (ZJUCEU2022015), and the Natural Science Foundation of Chongqing (CSTB2023NSCQ-MSX0950), all of which are greatly acknowledged by the authors

Conflict of interest

The authors declare that the research was conducted in the absence of any commercial or financial relationships that could be construed as a potential conflict of interest.

Publisher's note

Supplementary material

The Supplementary Material for this article can be found online at: https://www.frontiersin.org/articles/10.3389/fchem.2024.1413489/full#supplementary-material

References

Barnard, A. S., and Guo, H. (2011). Modeling the iron oxides and oxyhydroxides for the prediction of environmentally sensitive phase transformations. *Phys. Rev. B* 83 (9), 094112. doi:10.1103/physrevb.83.094112

Chen, G., Zhao, Y., Fu, G., Duchesne, P. N., Gu, L., Zheng, Y., et al. (2014). Interfacial effects in Iron-Nickel Hydroxide–Platinum nanoparticles enhance catalytic oxidation. *Science* 344, 495–499. doi:10.1126/science.1252553

Chen, Y., Lin, J., Li, L., Qiao, B., Liu, J., Su, Y., et al. (2018). Identifying size effects of Pt as single atoms and nanoparticles supported on FeO_x for the Water-Gas shift reaction. *ACS Catal.* 8 (2), 859–868. doi:10.1021/acscatal.7b02751

Dreyer, J. A. H., Grossmann, H. K., Chen, J., Grieb, T., Gong, B. B., Sit, P. H. L., et al. (2015). Preferential oxidation of carbon monoxide over Pt–FeO_x/CeO_2 synthesized by two-nozzle flame spray pyrolysis. *J. Catal.* 329, 248–261. doi:10.1016/j.jcat.2015.05.003

Gong, X., Hu, P., and Raval, R. (2003). The catalytic role of water in CO oxidation. *J. Chem. Phy.* 119 (12), 6324–6334. doi:10.1063/1.1602053

Haneda, M., Kawaguchi, Y., and Towata, A. (2017). CoO_x–FeO_x composite oxide prepared by hydrothermal method as a highly active catalyst for low-temperature CO oxidation. *J. Ceram. Soc. Jan.* 125 (3), 135–140. doi:10.2109/jcersj2.16219

Li, Q. R., Zhou, X. X., Zhao, W. P., Peng, C., Wu, H., and Chen, H. (2019). Pt/Fe co-loaded mesoporous zeolite beta for CO oxidation with high catalytic activity and water resistance. *RSC Adv.* 9 (48), 28089–28094. doi:10.1039/c9ra04599f

Li, R. Y., Zheng, X. H., Yan, H., Tuo, Y., Liu, Y., Feng, X., et al. (2024). Understanding the promotion effect of Pt in the reaction system of water gas shift reaction catalyzed by Pt/α-MoC from theoretical perspectives. *Appl. Surf. Sci.* 644, 158800. doi:10.1016/j.apsusc.2023.158800

Li, Z. H., Geng, Y., Ma, L., Chen, X., Li, J., Chang, H., et al. (2020). Catalytic oxidation of CO over Pt/Fe_3O_4 catalysts: tuning O_2 activation and CO adsorption. *Front. Env. Sci. Eng.* 14 (4), 65. doi:10.1007/s11783-020-1244-y

Lou, Y., and Liu, J. (2017). CO oxidation on metal oxide supported single Pt atoms: the role of the support. *Ind. Eng. Chem. Res.* 56 (24), 6916–6925. doi:10.1021/acs.iecr.7b01477

Ma, L., Chen, X. Y., Li, J. H., Chang, H., and Schwank, J. W. (2020). Electronic metal-support interactions in Pt/FeO_x nanospheres for O oxidation. *Catal. Today* 355, 539–546. doi:10.1016/j.cattod.2019.06.055

Nguyen, M., Seriani, N., and Gebauer, R. (2013). Water adsorption and dissociation on α-Fe_2O_3 (0001): PBE+U calculations. *J. Chem. Phy.* 138 (19), 194709. doi:10.1063/1.4804999

Oi-Uchisawa, J., Wang, S., Nanba, T., Ohi, A., and Obuchi, A. (2003). Improvement of Pt catalyst for soot oxidation using mixed oxide as a support. *Appl. Catal. B Environ.* 44 (3), 207–215. doi:10.1016/s0926-3373(03)00055-9

Onoe, T., Iwamoto, S., and Inoue, M. (2007). Synthesis and activity of the Pt catalyst supported on CNT. *Catal. Commun.* 8 (4), 701–706. doi:10.1016/j.catcom.2006.08.018

Rohrbach, A., Entel, P., and Hafner, J. (2004). First-principles calculation of the structure and magnetic phases of hematite. *Phy. Rev. B* 69 (16), 165107. doi:10.1103/physrevb.69.165107

Si, W. Z., Liu, H., Yan, T., Wang, H., Fan, C., Xiong, S., et al. (2020). Sn-doped rutile TiO_2 for vanadyl catalysts: improvements on activity and stability in SCR reaction. *Appl. Catal. B Environ.* 269, 118797. doi:10.1016/j.apcatb.2020.118797

Su, Z., Yang, W., Wang, C., Xiong, S., Cao, X., Peng, Y., et al. (2020). Roles of oxygen vacancies in the bulk and surface of CeO_2 for toluene catalytic combustion. *Environ. Sci. Technol.* 54 (19), 12684–12692. doi:10.1021/acs.est.0c03981

Tomita, A., Shimizu, K., and Tai, Y. (2014). Effect of metal oxide promoters on low temperature CO oxidation over Water-Pretreated Pt/Alumina catalysts. *Catal. Lett.* 144 (10), 1689–1695. doi:10.1007/s10562-014-1305-6

Wang, T., Xing, J., Zhu, L., Jia, A. P., Wang, Y. J., Lu, J. Q., et al. (2019). CO oxidation over supported Pt/$Cr_xFe_{2-x}O_3$ catalysts and their good tolerance to CO_2 and H_2O. *Appl. Catal. B Environ.* 245, 314–324. doi:10.1016/j.apcatb.2018.12.054

Xiong, S. C., Peng, Y., Wang, D., Huang, N., Zhang, Q., Yang, S., et al. (2020). The role of the Cu dopant on a Mn3O4 spinel SCR catalyst: improvement of low-temperature activity and sulfur resistance. *Chem. Eng. J.* 387, 124090. doi:10.1016/j.cej.2020.124090

Yang, W., Peng, Y., Wang, Y., Wang, Y., Liu, H., Su, Z., et al. (2020). Controllable redox-induced *in-situ* growth of MnO_2 over Mn_2O_3 for toluene oxidation: active heterostructure interfaces. *Appl. Catal. B Environ.* 278, 119279. doi:10.1016/j.apcatb.2020.119279

Zhang, Y. H., Wu, Y. D., Wang, H. F., Guo, Y., Wang, L., Zhan, W., et al. (2015). The effects of the presence of metal Fe in the CO oxidation over Ir/FeO_x catalyst. *Catal. Commun.* 61, 83–87. doi:10.1016/j.catcom.2014.12.018

Zhao, J., Lu, Z., He, X., Zhang, X., Li, Q., Xia, T., et al. (2017). Fabrication and characterization of highly porous $Fe(OH)_3$@ cellulose hybrid fibers for effective removal of Congo red from contaminated water. *ACS Sustain. Chem. Eng.* 5 (9), 7723–7732. doi:10.1021/acssuschemeng.7b01175

Zhao, Y., Chen, G., Zheng, N., and Fu, G. (2014). Mechanisms for CO oxidation on Fe(iii)–OH–Pt interface: a DFT study. *Faraday Discuss.* 176, 381–392. doi:10.1039/c4fd00144c

Zheng, B., Liu, G., Geng, L. L., Cui, J., Wu, S., Wu, P., et al. (2016). Role of the FeO_x support in constructing high-performance Pt/FeO_x catalysts for low-temperature CO oxidation. *Catal. Sci. Technol.* 6 (5), 1546–1554. doi:10.1039/c5cy00840a

Zhu, M. T., Zhang, K. F., Du, W. P., Jia, A. P., Luo, M. F., and Lu, J. Q. (2021). Highly active and water tolerant Pt/MFe_2O_4 (M = Co and Ni) catalysts for low temperature CO oxidation. *Appl. Catal. A Gen.* 619, 118142. doi:10.1016/j.apcata.2021.118142